Multi-Functional Light Emitter Based on Band-Edge Modes Near Γ-Point in Honeycomb Photonic Crystal

Po-Tsung Lee, *Member, IEEE*, Tsan-Wen Lu, and Kuan-Un Sio

***Abstract*—In this report, we demonstrate multi-functional light emitter based on band-edge modes near Γ-point in a two-dimensional honeycomb photonic crystal slab. Different band-edge modes near Γ-point are identified, including the monopole (Γ_2), dipole $(\Gamma_{4,5})$, and quadrupole $(\Gamma_{6,7})$ modes. The monopole and quadrupole modes lasing are observed with high side-mode suppression-ratio of 35 dB and high index sensitivity of 375 nm per refractive index unit, which shows their potential in optical micro-laser and index sensor applications. Over five-fold photoluminescence enhancement with broad band-width of 100 nm from the dipole mode is also observed at room temperature, which shows the advantage of honeycomb lattice structure for designing high brightness light emitting diodes.**

***Index Terms*—Enhanced light emission, honeycomb photonic crystal, optical sensor, semiconductor laser.**

I. Introduction

OVER past decades, the artificial photonic crystal (PhC) structures have been used to confine, guide, and extract photon flows in wavelength scale according to our desire for various optical components, including micro-laser sources, low-loss waveguides, and highly efficient light emitting diodes (LEDs), to construct photonic integrated circuits. Among these devices, the micro-lasers play important roles in a variety of technologies, including optical communication, information storage, sensor and imaging for biomedicine. In recent years, various two-dimensional (2-D) PhC cavity lasers [1]–[3] have shown the capability to confine photon flows in wavelength scale with very low losses by the photonic bandgap (PBG) effect.

Unlike the PhC cavity laser that confines photons in a defect region created inside the PhCs by the PBG effect, the PhC band-edge (BE) laser utilizes the flat photonic band with local group velocity $v_g \sim 0$ near high symmetric points to enhance light-gain interactions and achieves lasing operations [4]. Various 2-D PhC BE lasers with high- or low-index contrasts via optical or electrical driving have been investigated and demonstrated recently [5]–[8]. Generally, the BE modes can be classified into the slab-confined and radiative modes, whose frequencies lie below and above the light line, respectively. In a 2-D triangular PhC slab, the slab-confined BE modes are well-confined inside the slab and the lasing actions usually occur near M- and K-points with in-plane emissions [5]. In contrast, the lasing of radiative mode occurs near Γ-point with almost zero in-plane wave vector summation [9] and thus has directional surface laser emission with high output power. This feature is beneficial for micro-lasers and indicates high signal/noise (S/N) ratio for optical sensors. Because the BE mode lasing occurs in the PhC structure with large area and without delicate defect design, this type of device can be fabricated by high throughput fabrication processes with large fabrication tolerance, such as holographic lithography [10] and nano-imprint technologies [11].

In addition to the square and triangular PhCs, the honeycomb PhC with flat band-edge near Γ-point also attracts lots of attentions in serving as BE mode lasers [12]–[16] and other applications [17]–[20]. This lattice structure has lower air-filling factor than that of the square or triangular PhC because of less air holes, which leads to less non-radiative recombination, larger gain volume, and better heat dissipation. All of these are advantageous for active light emitting devices. However, up to date, most reports of honeycomb PhC lasers have focused on the lossy dipole mode with high threshold. Very few literatures

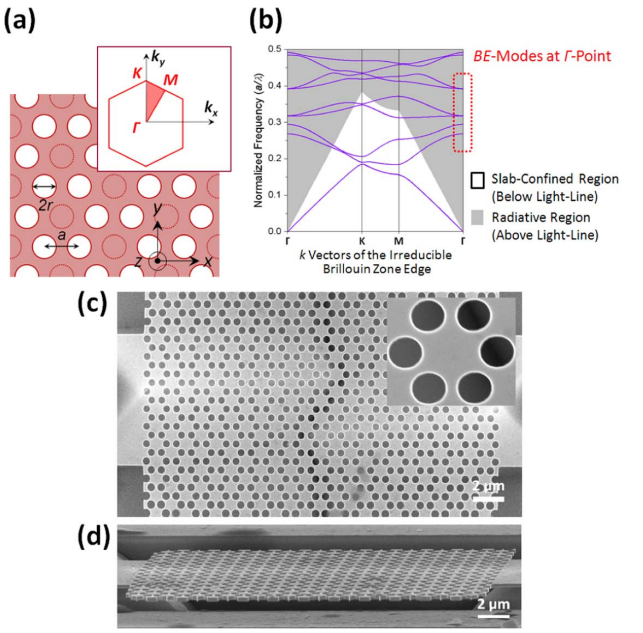

Fig. 1. (a) Scheme of the 2-D honeycomb PhC. The first and irreducible Brillouin zones are also shown as the inset. (b) TE-like band diagram of the 2-D honeycomb PhC slab by 3-D PWE simulation. (c) Top- and (d) tilted-view SEM pictures of the fabricated 2-D honeycomb PhC slab. The zoom-in SEM picture of a honeycomb PhC lattice cell is shown as the inset in (c).

Manuscript received November 16, 2010; revised February 18, 2011, March 31, 2011; accepted April 06, 2011. Date of publication May 02, 2011; date of current version May 27, 2011. This work was supported in part by Taiwan's National Science Council (NSC) under Contracts NSC-98-2221-E-009-015-MY2, NSC-99-2120-M-009-009, and NSC-100-3113-E-009-007-CC2.

The authors are with the Department of Photonics and Institute of Electro-Optical Engineering, National Chiao Tung University, Hsinchu 30010, Taiwan (e-mail: ricky.eo94g@nctu.edu.tw).

Digital Object Identifier 10.1109/JLT.2011.2142176

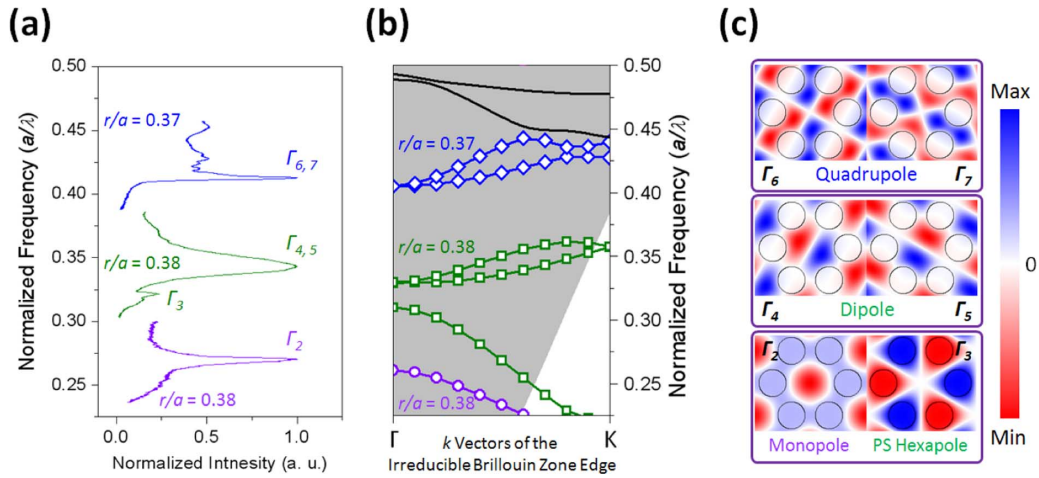

Fig. 2. (a) The measured spectra from the 2-D honeycomb PhC slabs with different lattice constants. (b) 3-D PWE simulated TE-like $\Gamma - K$ band diagram and (c) the simulated mode profiles in magnetic fields for modes from Γ_2 to Γ_7.

have investigated different BE modes near Γ-point in honeycomb PhC and their applications. In this report, we demonstrate and identify not only the dipole mode but also the monopole and quadrupole modes near Γ-point in a 2-D honeycomb PhC slab. We also demonstrate the multi-function of these BE modes in a 2-D honeycomb PhC slab, including micro-lasers, highly sensitive optical sensors, and broad band-width light emission enhancement.

II. BE Modes Near Γ-Point in 2-D Honeycomb PhC Slabs

The 2-D honeycomb PhC is obtained from the triangular lattice PhC with periodic missing air holes on a suspended InGaAsP slab shown in Fig. 1(a), where the refractive indexes of air and InGaAsP are set as 1.0 and 3.4, respectively. The air hole radius (r), lattice constant (a), first and irreducible Brillouin zones of the honeycomb PhC are defined in Fig. 1(a). For a 2-D honeycomb PhC slab with r/a ratio of 0.38 and slab thickness of $0.5a$, the corresponding transverse-electric-like (TE-like) band diagram is obtained by three-dimensional (3-D) plane-wave expansion (PWE) simulation, as shown in Fig. 1(b). In the following researches, we will focus on the BE modes near Γ-point as indicated in Fig. 1(b) with frequencies located in the shadow region above the light line, that is, the radiative region.

In fabrication, the epitaxial structure consisted of four 10 nm compressively strained InGaAsP multi-quantum-wells (MQWs) with 220 nm thickness grown on InP substrate is prepared. The silicon nitride layer as hard mask and the electron-beam resist for defining PhCs are deposited and spin-coated on the MQWs in sequence. The honeycomb PhCs are defined by electron-beam lithography on the resist layer. After a series of reactive ion etching and inductively coupled plasma dry-etching processes, the defined honeycomb PhCs are transferred into the MQWs. Finally, the slab structure is formed by diluted *HCl* wet-etching process. Top- and tilted-view scanning electron microscope (SEM) pictures of the 2-D honeycomb PhC slab with fabricated $a, r/a$, and device size of 640 nm, 0.40, and 23×14 lattice cells are shown in Figs. 1(c) and (d). The SEM picture of a honeycomb PhC lattice cell is also shown as the inset of Fig. 1(c).

All the fabricated devices are mounted on a 3 axis stage and optically pumped at room temperature by an 845 nm diode laser with pulsewidth and duty cycle of 25 ns and 0.75%. Via a $50\times$ objective lens with numerical aperture of 0.42, the excitation laser is focused to be a 10 μm spot in diameter on the devices. The emissions from the devices are collected vertically via the same objective lens, which are then fed into an optical fiber and analyzed by an optical spectrum analyzer with 50 pm spectral resolution. We observe different resonance peaks from the fabricated devices with different lattice constants at low excitation power, as shown in Fig. 2(a). Comparing these peaks with 3-D PWE simulated TE-like $\Gamma - K$ band diagram shown in Fig. 2(b), we can identify these peaks from low to high frequencies as Γ_2 (monopole mode), Γ_3 (phase-shifted (PS) hexapole mode), $\Gamma_{4,5}$ (dipole modes), and $\Gamma_{6,7}$ (quadrupole modes). The corresponding simulated mode profiles in magnetic fields are shown in Fig. 2(c). Among these modes, monopole and PS hexapole modes are non-degenerate modes and the others are degenerate modes. In addition to 3-D PWE method, we also perform 3-D finite-difference time-domain (FDTD) simulations with perfectly matched layer boundary condition to confirm that the PWE simulation results are reliable.

III. Emissions From BE Modes and Their Applications

According to the initial mode identifications from Figs. 2(a) and (b), the 2-D honeycomb PhC slabs with different parameters are fabricated and characterized for the monopole ($a = 420 - 450$ nm, $r/a = 0.38 - 0.44$) and quadrupole ($a = 620 - 650$ nm, $r/a = 0.38 - 0.44$) modes. The measured light-in light-out $(L - L)$ curves of laser emissions from sample-A ($a = 430$ nm, $r/a = 0.42$) and sample-B ($a = 640$ nm, $r/a = 0.38$) are shown in Figs. 3(a) and (b), which show lasing thresholds of 1.6 and 5.4 mW, respectively. The lasing spectra in dB scale of these two lasing modes both exhibit high side-mode suppression-ratio (SMSR) larger than 30 dB, as shown in Figs. 3(c) and (d). To further confirm the lasing modes as designed, the normalized monopole and quadrupole mode frequencies with different r/a ratios and fixed lattice constants obtained by 3-D PWE method are compared with the measured results, as shown

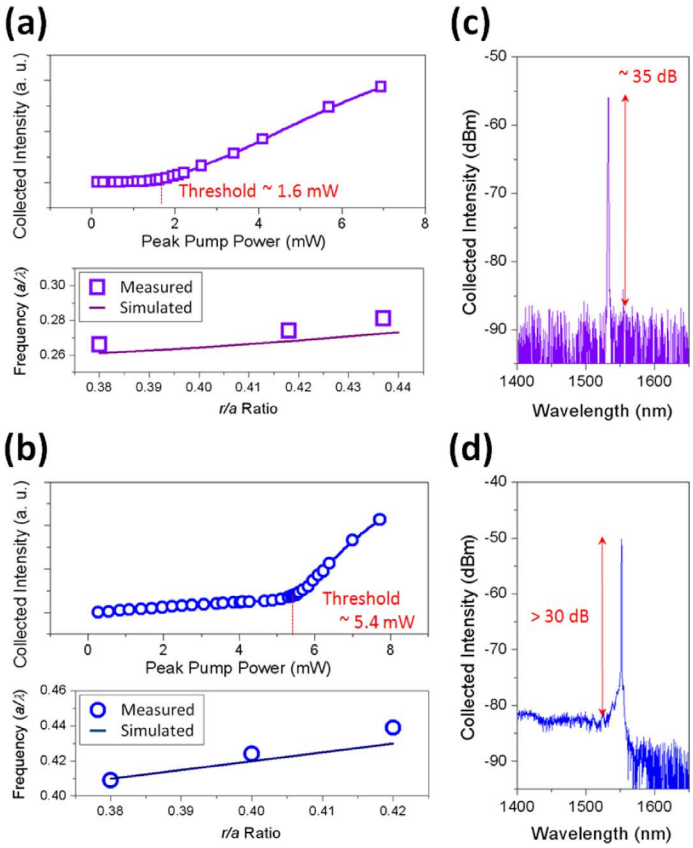

Fig. 3. (a)-(b) Measured $L-L$ curves and (c)–(d) lasing spectra in dB scale of lasing actions from the monopole and quadrupole modes. Mode identifications of the (a) monopole and (b) quadrupole modes by comparisons between the measured and 3-D PWE simulated results. The lattice constants in (a) and (b) are fixed at 430 and 650 nm, respectively.

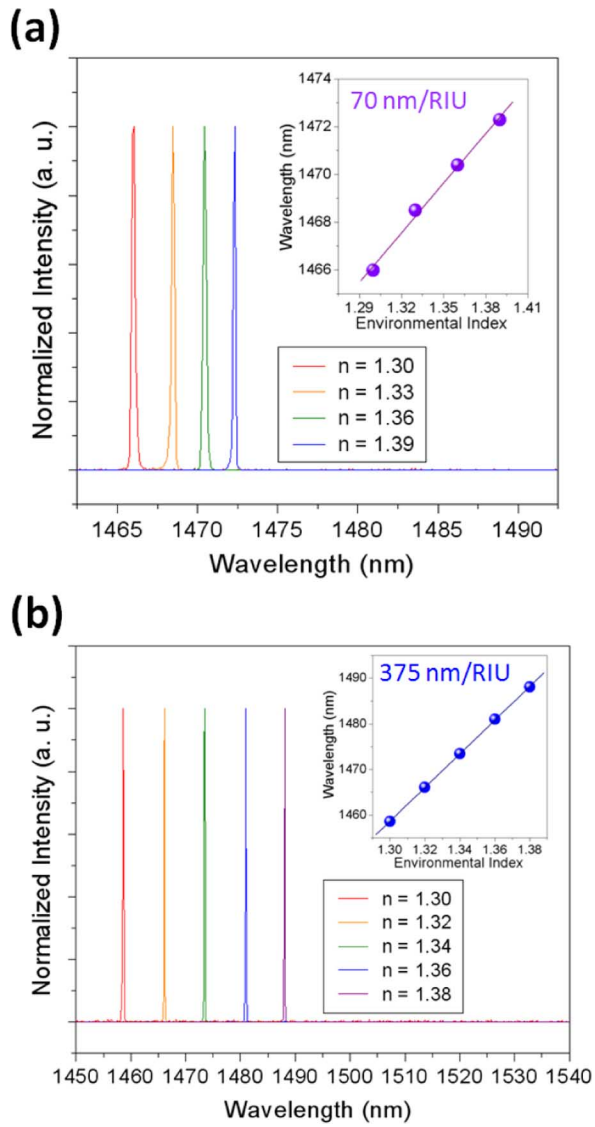

Fig. 4. The measured lasing spectra of the (a) monopole and (b) quadrupole modes with total index variations of 0.09 and 0.08, respectively. The wavelength shift fitting curves of the monopole and quadrupole modes are shown as the insets of (a) and (b) with the R_n values of 70 and 375 nm/RIU, respectively.

in Figs. 3(a) and (b). The good match indicates the lasing modes from sample-A and sample-B are the monopole and quadrupole modes, respectively. In addition, we perform 3-D FDTD simulations to calculate the quality (Q) factors of the monopole and quadrupole modes, which are 1 800 and 4 000, respectively. These lower Q factors than those of general PhC defect cavities are attributed to the radiative feature of the BE modes near Γ-point and the finite size of presented honeycomb *PhC slabs*. Thus, the lasing actions are mainly contributed from the enhanced light-gain interactions due to the BE slow light effect.

High SMSRs of the monopole and quadrupole modes not only meet the requirement for micro-lasers in optical communication systems but also indicate high S/N ratios when serving as optical sensors. To investigate the performances of these two lasing modes for optical sensing, we immerse the samples in different transparent index matching liquids (Cargille Labs) and obtain their lasing spectra, as shown in Figs. 4(a) and (b). In Fig. 4(a), for the monopole mode, we observe a wavelength shift of 6.3 nm under 0.09 refractive index variation from 1.30 to 1.39, which corresponds to an index sensitivity R_n of 70 nm per refractive index unit (nm/RIU). In Fig. 4(b), for the quadrupole mode, the wavelength shift reaches 30 nm under 0.08 refractive index variation from 1.30 to 1.38. Therefore, we obtain a relatively high R_n value of 375 nm/RIU from the quadrupole mode, which agrees with the simulated R_n value of 383 nm/RIU. This experimental R_n value from the quadrupole mode is much higher than those demonstrated by different PhC BE lasers [21], [22]. By considering the measured narrowest lasing spectral line-width of 0.13 nm, the minimum detectable index variation Δn_{det} is as low as 3.5×10^{-4}, which is comparable with those from carefully-designed PhC micro- and nano-cavities [23], [24] and much higher than those demonstrated by PhC BE lasers. This strongly shows that high R_n and small Δn_{det} can be achieved in this defect-free honeycomb PhC structure without delicate lattice tuning and purposive cavity design, which can be fabricated by high throughput fabrication processes. In addition, unlike the high Q cavities, due to the low Q factor of the BE mode near Γ-point, the low Q-dependence laser emission from the BE mode are also less sensitive to the absorptions and extra structural losses caused by different analytes [25], which could lead to a relatively stable sensing operation.

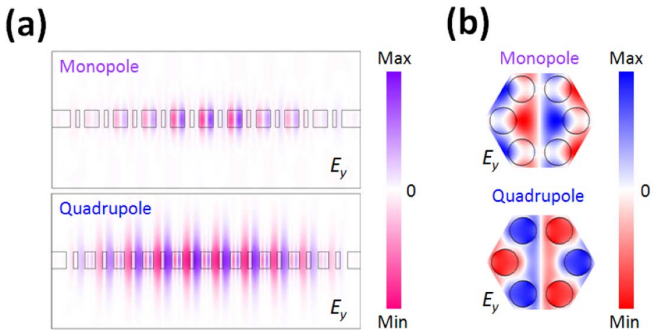

Fig. 5. (a) The 3-D FDTD simulated E_y fields of the monopole and quadrupole modes in honeycomb PhC slab in $x-z$ plane. (b) The 3-D PWE simulated E_y fields of the monopole and quadrupole modes in a honeycomb PhC cell in $x-y$ plane.

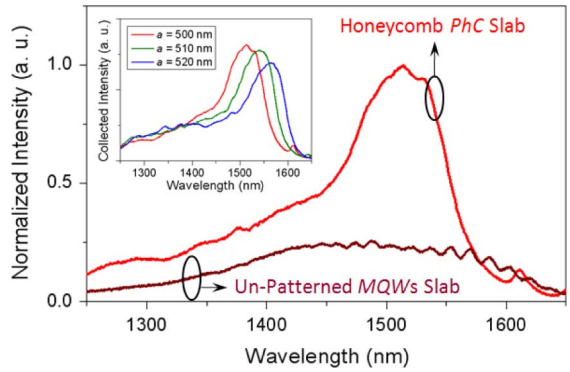

Fig. 6. The measured PL spectra from the 2-D honeycomb PhC and un-patterned MQWs slabs. Over five-fold PL enhancement near wavelength of 1510 nm attributed to the dipole mode near Γ-point is observed. The enhanced PL spectra under different lattice constants from 500 to 520 nm and fixed r/a ratio of 0.36 are also shown in the inset.

Because the simulated Q factors of the monopole and quadrupole modes are at the similar levels, the differences between the monopole and quadrupole modes in serving as micro-lasers and optical sensors can be understood by the 3-D FDTD simulated E_y fields in $x-z$ plane shown in Fig. 5(a). In Fig. 5(a), the E_y field of the monopole mode tends to distribute more in the dielectric region than that of the quadrupole mode. The 3-D PWE simulated E_y fields of the monopole and quadrupole modes in $x-y$ plane shown in Fig. 5(b) also agree with the 3-D FDTD simulation results. This difference in field distributions shows that the monopole mode has less radiation field extending into the air in z-direction and good mode field overlap with the dielectric gain region, which lead to lower lasing threshold of the monopole mode. As a result, the monopole mode is less sensitive to the environmental index variation, which leads to smaller R_n than that for the quadrupole mode for index sensing in experiments. Thus, we can conclude that the monopole and quadrupole modes in the 2-D honeycomb PhC slabs are suitable for micro-laser and optical sensor applications, respectively.

We also characterize the 2-D honeycomb PhC slab with $a = 500$ nm and $r/a = 0.36$ for the dipole mode. The measured spectrum is shown in Fig. 6. The mode is confirmed as the dipole mode by 3-D PWE simulations. Unlike the monopole and quadrupole modes, the lasing actions from the dipole mode are not observed. This is caused by the lossy feature of the dipole mode (the simulated Q is smaller than 100) and the poor excitation and collection efficiencies of the typical micro-photo-luminescence system under our available excitation power (<10 mW) [14]. Although the lasing action of the dipole mode is not observed, over five-fold photoluminescence (PL) enhancement compared to the un-patterned MQWs slab is obtained, as shown in Fig. 6. This enhancement is also attributed to the lossy feature of the dipole mode, which leads to much easier coupling of the mode energy into the air than the other modes. To further verify this PL enhancement from the dipole mode, the enhanced PL spectra of devices with different lattice constants from 500 to 520 nm are shown as the inset of Fig. 6. The red-shift of PL peak with increased lattice constant is observed and agrees with both 3-D PWE and FDTD simulation results. Moreover, the PL enhancement from the dipole mode is with broad band-width of 100 nm, which is broader than the monopole and quadrupole modes with narrow band-widths shown in Fig. 2. Thus, based on the dipole mode, we believe the honeycomb PhC structure with low air-filling factor is suitable to be applied to enhance light extraction for high brightness LEDs.

IV. Conclusion

In this report, we demonstrate multi-functional light emitter based on different BE modes near Γ-point in the 2-D honeycomb PhC slab. The monopole (Γ_2), dipole $(\Gamma_{4,5})$, and quadrupole $(\Gamma_{6,7})$ modes are observed in experiments and identified by 3-D PWE and FDTD simulations. We obtain the lasing actions from the monopole and quadrupole modes. The monopole mode lasing shows a low threshold of 1.6 mW and high SMSR of 35 dB because of good mode field overlap with the dielectric gain region, which is suitable as micro-lasers in optical communication systems. In contrast, the quadrupole mode lasing exhibits a high index sensitivity R_n of 375 nm/RIU and a very small Δn_{det} of 3.5×10^{-4} because the mode field tends to distribute in the environment, which has great potential for serving as highly sensitive optical bio-sensors. This also strongly shows that highly sensitive optical sensing can be achieved via such robust and defect-free honeycomb PhC without delicate nanocavity design, which can be fabricated by high throughput fabrication processes. Moreover, the presented honeycomb lattice with low air-filling factor shows over five-fold PL enhancement with broad band-width of 100 nm from the dipole mode at room temperature, which will be very beneficial for designing high brightness LEDs.

Acknowledgment

The authors would like to thank the help from Center for Nano Science & Technology (CNST) in National Chiao Tung University, Taiwan.

References

[1] H. G. Park, S. H. Kim, S. H. Kwon, Y. G. Ju, J. K. Yang, J. H. Baek, S. B. Kim, and Y. H. Lee, "Electrically driven single-cell photonic crystal laser," *Science*, vol. 305, pp. 1444–1447, 2004.

[2] K. Nozaki, S. Kita, and T. Baba, "Room temperature continuous wave operation and controlled spontaneous emission in ultrasmall photonic crystal nanolaser," *Opt. Exp.*, vol. 15, pp. 7506–7514, 2007.

[3] M. Nomura, N. Kumagai, S. Iwamoto, Y. Ota, and Y. Arakawa, "Photonic crystal nanocavity laser with a single quantum dot gain," *Opt. Exp.*, vol. 17, pp. 15975–15982, 2009.
[4] J. P. Dowling, M. Scalora, M. J. Bloemer, and C. M. Bowden, "The photonic band edge laser: A new approach to gain enhancement," *J. Appl. Phys.*, vol. 75, pp. 1896–1899, 1994.
[5] S. H. Kwon and Y. H. Lee, "High index-contrast 2-D photonic band-edge laser," *IEICE Trans. Electron.*, vol. E87, pp. 308–315, 2004.
[6] D. Ohnishi, T. Okano, M. Imada, and S. Noda, "Room temperature continuous wave operation of a surface-emitting two-dimensional photonic crystal diode laser," *Opt. Exp.*, vol. 12, pp. 1562–1568, 2004.
[7] A. Chen, S. J. Chua, G. C. Xing, W. Ji, X. H. Zhang, J. R. Dong, L. K. Jian, and E. A. Fitzgerald, "Two-dimensional AlGaInP/GaInP photonic crystal membrane lasers operating in the visible regime at room temperature," *Appl. Phys. Lett.*, vol. 90, p. 011113, 2007.
[8] H. Matsubara, S. Yoshimoto, H. Saito, Y. Jianglin, Y. Tanaka, and S. Noda, "GaN photonic-crystal surface-emitting laser at blue-violet wavelengths," *Science*, vol. 319, pp. 445–447, 2008.
[9] M. Imada, A. Chutinan, S. Noda, and M. Mochizuki, "Multidirectionally distributed feedback photonic crystal lasers," *Phys. Rev. B*, vol. 65, p. 195306, 2002.
[10] L. Wu, Y. Zhong, K. S. Wong, G. P. Wang, and L. Yuan, "Fabrication of hetero-binary and honeycomb photonic crystals by one-step holographic lithography," *Appl. Phys. Lett.*, vol. 88, p. 091115, 2006.
[11] V. Reboud, N. Kehagias, C. M. S. Torres, M. Zelsmann, M. Striccoli, M. L. Curri, A. Agostiano, M. Tamborra, M. Fink, F. Reuther, and G. Gruetzner, "Spontaneous emission control of colloidal nanocrystals using nanoimprinted photonic crystals," *Appl. Phys. Lett.*, vol. 90, p. 011115, 2007.
[12] Y. Park, S. Kim, C. Moon, H. Jeon, and H. J. Kim, "Butt-end fiber coupling to a surface-emitting Γ-point photonic crystal band edge laser," *Appl. Phys. Lett.*, vol. 90, p. 171115, 2007.
[13] F. Raineri, A. M. Yacomotti, T. J. Karle, R. Hostein, R. Braive, A. Beveratos, I. Sagnes, and R. Raj, "Dynamics of band-edge photonic crystal lasers," *Opt. Exp.*, vol. 17, pp. 3165–3172, 2009.
[14] G. Vecchi, F. Raineri, I. Sagnes, A. Yacomotti, P. Monnier, T. J. Karle, K. H. Lee, R. Braive, L. Le Gratiet, S. Guilet, G. Beaudoin, A. Taneau, S. Bouchoule, A. Levenson, and R. Raj, "Continuous-wave operation of photonic band-edge laser near 1.55 μm on silicon wafer," *Opt. Exp.*, vol. 15, pp. 7551–7556, 2007.
[15] C. M. Long, A. V. Giannopoulos, and K. D. Choquette, "Lateral current injection photonic crystal membrane light emitting diodes," *J. Vac. Sci. Technol. B*, vol. 28, pp. 359–364, 2010.
[16] S. Kim, Y. Park, K. Hwang, J. Lee, H. Jeon, and H. J. Kim, "High-power and large-alignment-tolerance fiber coupling of honeycomb-lattice photonic crystal Γ-point band-edge laser," *J. Opt. Soc. Am. B*, vol. 26, pp. 1330–1333, 2009.
[17] M. Yan, P. Shum, and J. Hu, "Design of air-guiding honeycomb photonic bandgap fiber," *Opt. Lett.*, vol. 30, pp. 465–467, 2005.
[18] R. Gajić, R. Meisels, F. Kuchar, and K. Hingerl, "All-angle left-handed negative refraction in Kagomé and honeycomb lattice photonic crystals," *Phys. Rev. B*, vol. 73, p. 165310, 2006.
[19] M. Bahriz, V. Moreau, R. Colombelli, O. Crisafulli, and O. Painter, "Design of midIR and THz quantum cascade laser cavities with complete TM photonic bandgap," *Opt. Exp.*, vol. 15, pp. 5948–5965, 2007.
[20] P. Ma, F. Robin, and H. Jäckel, "Realistic photonic bandgap structures for TM-polarized light for all-optical switching," *Opt. Exp.*, vol. 14, pp. 12794–12802, 2006.
[21] L. Ferrier, O. El Daif, X. Letartre, P. R. Romeo, C. Seassal, R. Mazurczyk, and P. Viktorovitch, "Surface emitting microlaser based on 2-D photonic crystal rod lattices," *Opt. Exp.*, vol. 17, pp. 9780–9788, 2009.
[22] S. Kim, J. Lee, H. Jeon, and H. J. Kim, "Fiber-coupled surface-emitting photonic crystal band edge laser for biochemical sensor applications," *Appl. Phys. Lett.*, vol. 94, p. 133503, 2009.
[23] S. Kita, K. Nozaki, and T. Baba, "Refractive index sensing utilizing a cw photonic crystal nanolaser and its array configuration," *Opt. Exp.*, vol. 16, pp. 8174–8180, 2008.
[24] T. W. Lu, Y. H. Hsiao, W. D. Ho, and P. T. Lee, "High-index sensitivity of surface mode in photonic crystal hetero-slab-edge microcavity," *Opt. Lett.*, vol. 35, pp. 1452–1454, 2010.
[25] S. Tomljenovic-Hanic, A. Rahmani, M. J. Steel, and C. M. de Sterke, "Comparison of the sensitivity of air and dielectric modes in photonic crystal slab sensors," *Opt. Exp.*, vol. 17, pp. 14552–14557, 2009.

Po-Tsung Lee (M'06) received the B.S. degree from the Department of Physics, National Taiwan University (NTU), Taipei, Taiwan, in 1997 and the M.S. and Ph.D. degrees from the Department of Electrical Engineering-Electrophysics, University of Southern California (USC), Los Angeles, USA, in 1998 and 2003, respectively. During the Ph.D. study, she was engaged in photonic crystal microcavity lasers. Prof. Lee was the recipient of the University of Southern California Women in Science and Engineering (WISE) Award in 2000–2001.

In 2003, she joined the Institute of Electro-Optical Engineering, National Chiao Tung University (NCTU), Hsinchu, Taiwan, as an Assistant Professor. In 2007, she became an Associate Professor in the Department of Photonics, NCTU. Her recent research interests are III-V semiconductor photonic crystal active and passive devices and their applications, organic memory, and silicon-based solar-cell technologies.

Tsan-Wen Lu received the B.S. degree from the Department of Electrical Engineering, National Tsing Hua University (NTHU), Hsinchu, Taiwan, in 2003. He then received the M.S. and Ph.D. degrees from the Institute of Electro-Optical Engineering, National Chiao Tung University (NCTU), Hsinchu, Taiwan, in 2005 and 2009, respectively. Currently, Dr. Lu holds a post-Dr. fellowship in NCTU. His recent research interests are surface modes in photonic crystal slab-edge and photonic crystal light-emitting devices for optical bio-sensing.

Kuan-Un Sio received the B.S. degree from the Department of Physics, National Taiwan Normal University (NTNU), Taipei, Taiwan, in 2008 and the M.S. degree from the Institute of Electro-Optical Engineering, National Chiao Tung University (NCTU), Hsinchu, Taiwan, in 2010. His research was focused on electrically-driven photonic crystal light emitters. Currently, he is a process engineer in Taiwan Semiconductor Manufacturing Company (TSMC), Hsinchu, Taiwan.